Vanselow, Christoph ; Fischer, Andreas

Influence of inhomogeneous refractive index fields on particle image velocimetry

Journal Article as: peer-reviewed accepted version (Postprint)

DOI of this document*(secondary publication): https://doi.org/10.26092/elib/3313

Publication date of this document: 13/09/2024

* for better findability or for reliable citation

Recommended Citation (primary publication/Version of Record) incl. DOI:

Christoph Vanselow, Andreas Fischer, Influence of inhomogeneous refractive index fields on particle image velocimetry, Optics and Lasers in Engineering, Volume 107, 2018, Pages 221-230, ISSN 0143-8166, https://doi.org/10.1016/j.optlaseng.2018.03.020.

Influence of inhomogeneous refractive index fields on particle image velocimetry

Christoph Vanselow*, Andreas Fischer

Bremen Institute for Metrology, Automation and Quality Science (BIMAQ), University of Bremen, Linzer Str. 13, Bremen 28359, Germany

ARTICLE INFO

Keywords:
Particle image velocimetry
Refractive index
Measurement error
Hot jet flow

ABSTRACT

The influence of inhomogeneous refractive index fields on particle image velocimetry (PIV) measurements is a well known problem, which leads to an unknown measurement uncertainty in, e.g., flame flows, shock waves and super sonic flows. Previous studies give only rough estimations of the measurement error due to inhomogeneous refractive index fields, and quantitative information is only available for special conditions such as a gradient of the refractive index independent of the viewing direction. Hence, the assessment of the spatial distribution of the quantitative measurement errors inside inhomogeneous refractive index distributions especially for stereoscopic and tomographic PIV is an open question. For this purpose, the flow measurement inside a hot jet flow is considered as an example, and a general analytic description of the error of the measured particle positions inside the hot jet flow is derived, numerically evaluated and finally validated by experiments. In particular, the determination of the particle position with triangulation is investigated, which is performed in stereoscopic and tomographic PIV. As a result, the measurement error is generally larger than for standard PIV without triangulation. The theoretically predicted errors of the measured particle position are validated with experiments and here amount to 11.7 μm for standard PIV and 17.3 μm for triangulation at the same distance from the center of the flow, respectively. Note that the error estimation requires the knowledge of the refractive index field that was determined by temperature measurements in the flow. Furthermore, the error analysis shows that for triangulation the measured particle position depends on the gradient and the curvature of the refractive index field, whereas for standard PIV the measured particle position only depends on the gradient of the refractive index. For the given temperature profile with a maximum temperature of 191 °C, the resulting flow velocity error is maximally 0.8 % with standard PIV, 1.7 % for the in plane and 2.9 % for the out of plane direction with stereoscopic PIV and 1.1 % with triangulation which is performed in tomographic PIV.

1. Introduction

Particle image velocimetry (PIV) is a well established technique for the measurement of fluid dynamics [1]. While the standard PIV principle allows the measurement of two velocity components, the stereoscopic and tomographic PIV approach provide three component velocity vectors in the image plane or volume [12,15] by considering the information of two or more additional camera perspectives. Including the information of further camera images is accompanied by the difficulty of determining the relation between these images. Thus a precise calibration of the imaging setup is inevitable and a crucial point for the measurement's feasibility and accuracy [2,8]. Determining the mapping functions, which correlate the 2D images with the world coordinates, allows the usage of the additional information from further camera perspectives.

The influence of inhomogeneous refractive index distributions leads to aberrations in the camera images and results in an increased measurement uncertainty for PIV measurements. Impacts on standard PIV measurement for turbulent flames are studied by Stella et al. [19]. In premixed flames the major influence on the refractive index are temperature disparities. The inhomogeneous refractive index causes a light sheet deflection and an image distortion but no quantitative information about the PIV measurement uncertainties are given. Elsinga et al. [5] use the background oriented schlieren (BOS) technique [14] to quantify the optical distortions arising from refractive index fields. The information about optical distortions are used to correct the measured velocity field of a compressible supersonic flow with the assumption of a gradient of the refractive index distribution independent of the viewing direction. The BOS technique measures the errors of an imaged known pattern placed in the background of the refractive index field. Therefore, the information about the refractive index field is limited to summed light deflections between the camera and the pattern placed in the background. Thus, for quantitative information about occurring PIV measurement errors inside the inhomogeneous refractive index field further information about the refractive index field, e.g., symmetric conditions are required.

* Corresponding author.
E-mail address: c.vanselow@bimaq.de (C. Vanselow).

Furthermore, a time resolved correction of image distortions was recently demonstrated for micro PIV by Koukourakis et al. using a spatially distributed Fresnel guide star [7]. However, the approach with adaptive optics is limited to slowly varying distortions due to the response time of the used spatial light modulator. Furthermore, the technique requires the knowledge of the spatial frequencies and amplitudes of the occurring image distortions. For this reason, similar corrections for PIV measurements inside refractive index distributions such as in hot jet flows, flame flows or shock waves, i.e., flows with non-constant temperature, pressure, fluid phase or fluid material, are difficult or impossible especially for fluctuating phenomena [5,16,19]. The consequence is an increase of the PIV measurement uncertainty.

As a result, the influence of refractive index variations on standard PIV measurements was addressed in several studies, but a remaining basic problem is to give quantitative information about the uncertainties. This holds true especially for stereoscopic and tomographic PIV measurements and for measurements inside complex flows with an inhomogeneous refractive index distribution. In contrast to standard PIV, for stereoscopic and tomographic PIV further difficulties occur with respect to the different particle position errors for the optical paths from the measurement region to each of the cameras.

The stereoscopic and tomographic techniques are based on different evaluations. Stereoscopic PIV uses the cross-correlated time dependent displacement of the particle patterns of each camera. The spatial resolution in PIV measurements is achieved by subdividing the measurement volume. Due to different errors in the cameras images, the sub volumes of each camera are consequently shifted to each other. Thus, an increase in the measurement uncertainty of the velocity has to be expected. Static refraction problems caused by for example optical windows can be taken into account [13,17] for stereoscopic PIV. Even unknown static optical distortion can be corrected by placing a well known calibration plate into the interrogation area to quantify image distortions. However, the correction techniques cannot be applied to dynamic changes of the refractive index, e.g., in flames or shock waves. For a tomographic reconstruction of the particle distribution, the lines of sight of the particle images on each camera have to intersect for a registration of the particle and its position. Uncertainties smaller than the diameter of the particle lead to a decrease of the quality of the reconstructed particle distribution [4]. Wieneke proposed self calibration procedures for stereoscopic [24] and tomographic [25] PIV to correct misalignment of the mapping functions. The stereoscopic self-calibration determines a disparity map by performing the cross-correlation of particle images of each camera at an identical time. The disparity map is zero for the case of perfect mapping functions. Any discrepancies in the disparity map can be interpreted as a misalignment of the light sheet plane and the coordinate system of the mapping function of each camera. The offset can be determined by solving the triangulation problem for each particle. The parameters of a plane fit through the resulting offsets can be used to correct the mapping functions. Similar to the stereoscopic procedure, the tomographic self-calibration also uses particle images to determine a disparity map which is used to correct the mapping functions. In either case, problems can occur for asymmetric image distortions, which result in a false correction of every mapping function. The consideration of estimated measurement errors caused by refractive index distributions provides the possibility to perform a superior correction of the mapping functions.

For this reason, the paper analyzes the occurring measurement errors for standard, stereoscopic and tomographic PIV measurements due to inhomogeneous distributions of the refractive index by simulation and experiment. In Section 2, a model is described for the determination of an inhomogeneous refractive index field caused by an inhomogeneous temperature distribution. The validation of this model is achieved by a comparison of the simulated and experimentally measured light ray deflection for the light ray propagation through air with an inhomogeneous temperature field. In Section 3, an analytic expression for the PIV measurement error of the particle position is derived, which allows the determination of particle position errors inside inhomogeneous refractive index distributions. Furthermore, the implications for the triangulation error in stereoscopic and tomographic PIV measurements are specified. In Section 4, the computational results are compared to experimentally determined particle position errors. The location dependent particle position error leads to an error of the determined velocity, which is quantified in Section 5.

2. Light deflection by inhomogeneous refractive index distributions

Light ray deflection occurs inside inhomogeneous refractive index distributions. A calculation of the particle displacement in PIV measurements caused by light deflection requires a reliable model for the refractive index n in dependency of the varying influencing quantities. Various influences such as the density $\rho(\vec{r})$ at the position $\vec{r} = (x, y, z)$ of the optical media affect the refractive index $n(\vec{r})$. Here, density variations caused by a hot jet flow are examined due to occurring light ray deflection. The Gladstone–Dale equation [11]

$$n(\vec{r}) - 1 = K\rho(\vec{r}) \propto \frac{K}{1 + \gamma(T(\vec{r}) - T_0)} \tag{1}$$

is used to determine the refractive index field referring to the temperature distribution of the air flow, where $K = 2.3 \cdot 10^{-4}$ is the Gladstone–Dale constant for air. The proportionality of the density is described by the law of Gay–Lussac and depends on the coefficient of thermal expansion γ, the temperature $T(\vec{r})$ and the reference temperature $T_0 = 293\,\mathrm{K}$. Assuming an ideal gas, the coefficient of thermal expansion is $\gamma = \frac{1}{T_0}$. The temperature is also the dominant factor for the refractive index distribution in premixed combustion, whereas in non-premixed hydrocarbon flames the Gladstone–Dale constant shows variations up to 100 % [18]. Thus, Eq. (1) is also applicable for premixed combustion with an adaption of the Gladstone–Dale constant. For a measured temperature distribution $T(\vec{r})$, ray tracing simulations can be used to calculate the light ray deflection by solving the fundamental equation for the propagation of light [3]

$$\frac{\mathrm{d}}{\mathrm{d}s}\left(n(\vec{r})\frac{\mathrm{d}\vec{r}}{\mathrm{d}s}\right) = \vec{\nabla}n(\vec{r}), \tag{2}$$

where ds is the optical path element. The direction of the light propagation depends on the gradient of the refractive index, i.e., the light beam deflects towards the optically denser medium.

A validation of Eq. (1) is achieved by a comparison of the simulated and the experimentally measured deflection angles α_x in x-direction, cf. the setup depicted in Fig. 1a. The test object is a hot jet flow, that is provided by a hot air gun. The cross section at $y = 2$ cm and $z = 0$ cm of the temperature profile was measured by a thermocouple, where the coordinate origin is set to the center of the nozzle exit with a diameter of $d_{\mathrm{nozzle}} = 4.2$ cm and the y-axis is parallel to the flow direction. The assumption of a radial symmetric flow condition allows an extrapolation for the 2D temperature profile at $y = 2$ cm. The obtained temperature distribution $T(x, y = 2\,\mathrm{cm}, z)$ perpendicular to the nozzle main flow direction is depicted in Fig. 1b. The arising beam shift dx on a screen at the distance $d = 132$ cm is measured with a camera. The resulting light ray deflection is acquired for varied positions of the laser in x-direction and the deflection angle is determined by $\tan\alpha_x = \frac{dx}{d}$. The mean deflection angle of 100 measurements and the results from the ray tracing simulation are shown in Fig. 2.

The comparison shows a good agreement of the simulated and the measured light ray deflection. The simulated data is confirmed by the measurement within a coverage factor of k=3 for the uncertainty of the mean values. Minor discrepancies occur in the outer region of the temperature distribution. The deviations between the simulation and the measurement results are caused by temperature measurement errors. A

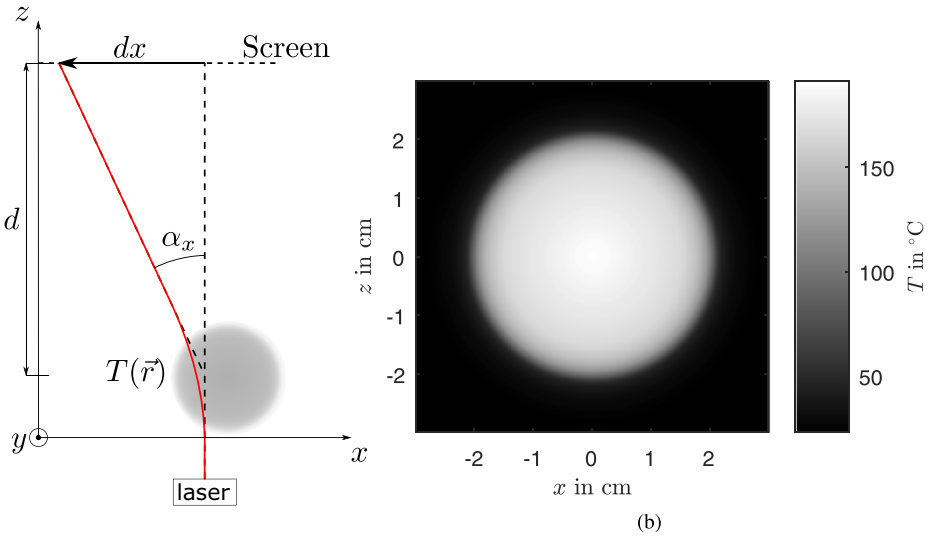

Fig. 1. (a) Experimental setup for the measurement of the light ray defection at $y = 2$ cm. The coordinate origin is the center of the nozzle exit. A laser beam is directed to a screen imaged with a camera. The light ray is moved in x-direction through a hot jet flow with the temperature distribution $T(\vec{r})$. The resulting deflection angle α_x in x-direction is determined by the shift dx of the laser spot on the screen at the distance $z = d$ from the center of the hot jet flow. (b) The measured mean temperature profile of the hot jet flow by thermocouple at $y = 2$ cm.

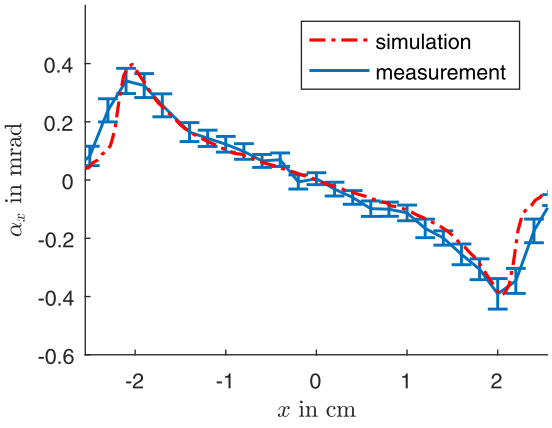

Fig. 2. Comparison of the measured and the simulated deflection angle α_x of the light beam propagating through the temperature distribution caused by the hot jet flow.

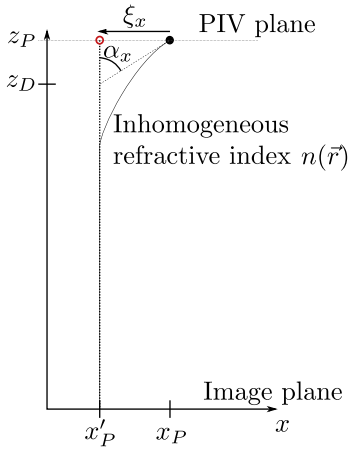

Fig. 3. The displacement ξ_x of the measured particle position $\vec{r}_{\mathrm{P}'} = (x_{\mathrm{P}'}, z_{\mathrm{P}})$ to the correct particle position $\vec{r}_{\mathrm{P}} = (x_{\mathrm{P}}, z_{\mathrm{P}})$ occurs by light deflection caused by an inhomogeneous refractive index distribution $n(\vec{r})$.

misalignment of the temperature measurement with respect to the nozzle center leads to measurement errors particularly in the outer regions of the simulated light ray deflection due to the locally increased temperature gradients. Apart from that, the agreement of deflection angles in the center of the flow between the measurement and the ray tracing simulation validate Eq. (1), which allows the determination of measurement errors for PIV measurements influenced by inhomogeneous refractive index distributions caused by temperature fields.

3. Uncertainty evaluation for PIV

As light ray deflection inside temperature fields can now be simulated, a theoretical description for a quantitative estimation of the expected measurement errors for PIV measurements inside refractive index distributions follows. The measurement error of the particle position $\vec{r}_{\mathrm{P}} = (x_{\mathrm{P}}, y_{\mathrm{P}}, z_{\mathrm{P}})$ inside a refractive index field is investigated at first for standard PIV with a single camera, see Fig. 3. For a simpler visualization, the light ray deflection is reduced to a two dimensional case. The light ray from a particle imaged by the camera is deflected, which leads to a measurement error for the particle position $\vec{r}_{\mathrm{P}} = (x_{\mathrm{P}}, y_{\mathrm{P}}, z_{\mathrm{P}})$. The camera 'sees' the particle at the position $\vec{r}_{\mathrm{P}'} = (x_{\mathrm{P}'}, y_{\mathrm{P}'}, z_{\mathrm{P}})$, which is the intersection of the line of sight of the camera and the PIV plane. The error $\vec{\xi} = \vec{r}_{\mathrm{P}} - \vec{r}_{\mathrm{P}'}$ of the measured particle position is the difference between the particle's true position and the measured position while the z-coordinate z_{P} is defined by the light sheet position.

Using Eq. (2), the particle position error can be determined. In order to prevent the necessity to perform a ray tracing simulation for each particle, an analytic expression for the error $\vec{\xi}$ of the particle location is derived. In addition, the analytic expression allows to identify fundamental dependencies of the measurement error for PIV measurements.

The error of the measured particle position depends on the deflection angle $\vec{\alpha} = (\alpha_x, \alpha_y, \alpha_z)$ and is provided by Merzkirch et al. [11] as

$$\vec{\xi} = (z_{\mathrm{P}} - z_{\mathrm{D}}) \tan\vec{\alpha} = (z_{\mathrm{P}} - z_{\mathrm{D}}) \int_0^{z_{\mathrm{P}}} \frac{1}{n(\vec{r})} \vec{\nabla} n(\vec{r}) \mathrm{d}z, \tag{3}$$

where $z_{\mathrm{P}} - z_{\mathrm{D}}$ is the distance between the point of intersection of the line of sight of the camera and the straight line from the true particle position in the direction of the deflected light ray, cf. Fig. 3. In Eq. (3),

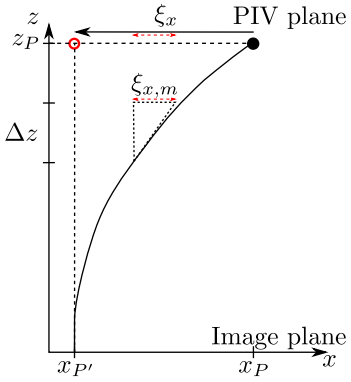

Fig. 4. The distance z_p is divided in intervals Δz to determine the error of the measured particle position ξ_x by the sum of N gradient triangles $\xi_{x,m}$, $m = 1, 2, \ldots, N$.

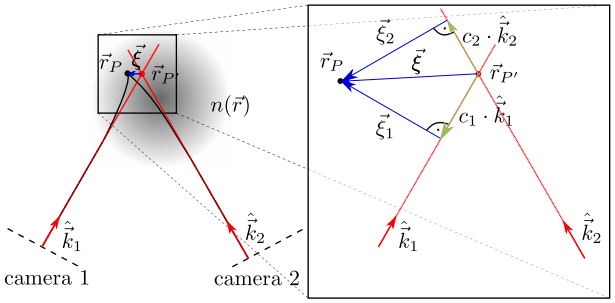

Fig. 5. The triangulation problem for a particle image pair acquired by two cameras in an inhomogeneous refractive index field. The error $\vec{\xi}$ of the measured particle location $\vec{r}_{P'}$ to the true position $\vec{r}_\mathrm{p}$ is correlated to the error $\vec{\xi}_1$ and $\vec{\xi}_2$ of each camera. The particle position is determined by the intersection of the lines of sight $\hat{\vec{k}}_1$ and $\hat{\vec{k}}_2$ of the cameras. The error $\vec{\xi}$ equals the vectorial addition of $\vec{\xi}_i$ and $c_i\hat{\vec{k}}_i$ for the ith camera with the coefficient c_i.

the approximation $\mathrm{d}s \approx \mathrm{d}z$ is applied which is justified for small errors. However, the position z_D is generally unknown. For this reason, the error $\vec{\xi}$ is approximated by a sum of N gradient triangles with the distance $\Delta z = \frac{z_\mathrm{p}}{N}$, see Fig. 4,

$$\vec{\xi} = \sum_{m=0}^{N} \vec{\xi}_{m+1} = \Delta z \sum_{m=0}^{N} \int_0^{m\Delta z} \frac{1}{n\left(\vec{r}\right)} \vec{\nabla} n\left(\vec{r}\right) \mathrm{d}z. \tag{4}$$

Note that Eq. (4) can be solved with a cumulative sum to save computation time and to get a distance dependent position error $\vec{\xi}_m(x, y, z = m \cdot \Delta z)$. Furthermore, the unknown parameter z_D from Eq. (3) is eliminated. This leads to the solvability of the location dependent particle position error for a given refractive index field.

3.1. Implications for triangulation error

According to the result in Eq. (4) for standard PIV, the error of the measured particle position depends on the line of sight of the camera. A reconstruction of the 3D particle location needs generally more than one camera. The particle location is triangulated by the intersection of the lines of sight allocated by the displayed particle. For large distortions in the particle images, the lines of sight disperse, which can lead to the loss of the particle in the tomographic reconstruction procedure. In case of a successfully reconstructed particle position inside an inhomogeneous refractive index field, the error of the measured particle position depends on the individual errors $\vec{\xi}_i$ of the cameras, where the index i denotes the camera number. The errors $\vec{\xi}_i$ are generally different due to the different optical paths. Thus, the correct particle location is unknown. In the following, the geometrical problem is investigated to give quantitative information about the error of the measured particle position. In Fig. 5, a diagram of the errors for the case of a two camera setup is depicted. Again, for better visualization, the diagram shows a two dimensional problem. However, the derived theoretical description also holds true for the three dimensional case. According to the geometric quantities introduced in Fig. 5, the measurement error $\vec{\xi}$ of the particle at the position $\vec{r}_\mathrm{p}$ is

$$\vec{\xi} = \vec{\xi}_i + c_i \hat{\vec{k}}_i, \tag{5}$$

where c_i is a scaling factor of the line of sight $\hat{\vec{k}}_i$ representing the line of sight of each camera imaging the particle. As the coefficients c_i are unknown, the coefficient c_1 is calculated by equating the two cases $i = 1, 2$ for Eq. (5). For the three dimensional problem one gets three equations with two unknowns c_1 and c_2. Eliminating c_2 by using the equations for the dimensions x and z results in

$$c_1 = \frac{\Delta\xi_x - \frac{k_{2,x}}{k_{2,z}} \cdot \Delta\xi_z}{k_{1,z} \cdot \left(\frac{k_{2,x}}{k_{2,z}} - \frac{k_{1,x}}{k_{1,z}}\right)} \tag{6}$$

with $\Delta\vec{\xi} = \vec{\xi}_1 - \vec{\xi}_2$. Inserting Eq. (6) into Eq. (5) leads to an expression for the triangulation error due to the influence of inhomogeneous media. The error only depends on the lines of sight $\hat{\vec{k}}_1$ and $\hat{\vec{k}}_2$ and the individual errors $\vec{\xi}_1$ and $\vec{\xi}_2$ in the camera images which are given by Eq. (4).

The results show that, the absolute error $|\xi|$ is larger or equal to the individual error $|\xi_i|$ referring to standard PIV measurements

$$|\vec{\xi}| \geq |\vec{\xi}_i|, \tag{7}$$

since the individual error is perpendicular to the line of sight, cf. Eq. (5). Furthermore, due to the singularity in the denominator in Eq. (6), the error $\vec{\xi}$ increases for

$$\left(\frac{k_{2,x}}{k_{2,z}} - \frac{k_{1,x}}{k_{1,z}}\right) \to 0. \tag{8}$$

The fraction $\frac{k_x}{k_z}$ is the slope of the line of sight. Since similar slopes for both cameras are obtained for the case of sharp angles between the cameras, the error of the measured particle position is expected to increase for sharp angles between the cameras.

In contrast to Eq. (4) (standard PIV), the triangulation error according to Eqs. (5) and (6) contains differences $\Delta\vec{\xi}$ of the individual errors $\vec{\xi}_i$ of the measured particle position. For further quantification and interpretation of the triangulation error, Eq. (4) can be used to determine the difference

$$\Delta\vec{\xi} = \Delta z \sum_{m=0}^{N} \int_0^{i\Delta z} \left[\frac{\vec{\nabla} n\left(\vec{r}_1(z)\right)}{n\left(\vec{r}_1(z)\right)} - \frac{\vec{\nabla} n\left(\vec{r}_2(z)\right)}{n\left(\vec{r}_2(z)\right)}\right] \mathrm{d}z. \tag{9}$$

Here, $\vec{r}_1(z) = (x_1(z), y_1(z), z)^T$ and $\vec{r}_2(z) = (x_2(z), y_2(z), z)^T$ define the optical paths for the cameras 1 and 2. Using the difference quotient and the quotient rule of the differential calculus, Eq. (9) can also be written in the form

$$\Delta\vec{\xi} = \Delta z \sum_{m=0}^{N} \int_0^{i\Delta z} \int_{\vec{r}_1(z)}^{\vec{r}_2(z)} \left[\frac{\vec{\nabla}^2 n\left(\vec{r}\right)}{n\left(\vec{r}\right)} - \frac{\left(\vec{\nabla} n\left(\vec{r}\right)\right)^2}{n^2\left(\vec{r}\right)}\right] d\vec{r}\,\mathrm{d}z. \tag{10}$$

Hence, the error of the particle position, which is determined with triangulation, not only depends on the gradient but also on the curvature of the refractive index.

4. Experimental validation

The theoretical results described in Section 3 are validated by the comparison with experimental measurements. In order to examine the

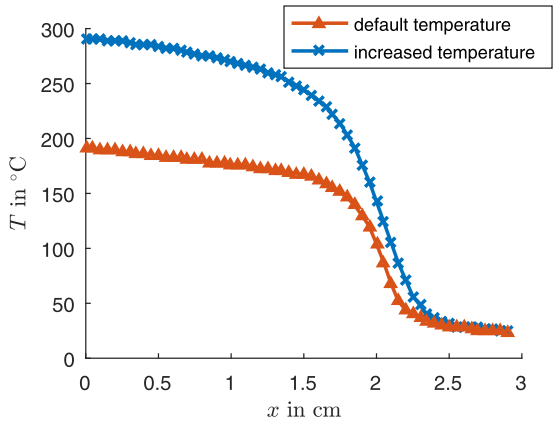

Fig. 6. Comparison between the default (red line) and increased (blue line) temperature profile at $y = 2$ cm and $z = 0$ cm. (For interpretation of the references to colour in this figure legend, the reader is referred to the web version of this article.)

particle position error inside inhomogeneous refractive index distributions, the ending of a single mode glass fiber is inserted into the hot jet flow and depicted by a camera with a line of sight in positive z-direction. The position of the fiber in the camera image is determined by the arithmetic mean of the pixels depicting the fiber weighted by the intensity. A fiber diameter of a few micrometers is suitable to imitate the light source of an illuminated particle. The relative position of the glass fiber ending to the jet is varied by a linear stage in x-direction at $y_{\text{fiber}} = 2$ cm above the nozzle exit. To prove the validity of the proposed calculation method for the position error inside inhomogeneous refractive index distributions (Eq. (4)), two different measurement setups are considered.

First, two different temperature distributions are used in order to validate the model for different temperature ranges, which are provided by the hot air gun with different heat powers. In Fig. 6 the measured default temperature profile (red line), which results in the temperature distribution shown in Fig. 1(b), is compared to the increased temperature profile (blue line) in x-direction from the center of the flow for $y = 2$ cm. The increased temperature of the hot jet flow with a maximum of 291 °C also has an increased flow velocity. Second, the position in z-direction is arbitrary chosen by $z_{\text{fiber1}} = 1.3$ cm in the default flow and $z_{\text{fiber2}} = 3.3$ cm in the flow with increased temperature in order to validate the location dependency of the calculated particle position error.

And third, the diameter of the single mode fiber is varied from $d_{\text{fiber1}} = 3.4$ µm in the default flow to $d_{\text{fiber2}} = 2.5$ µm in the flow with increased temperature to analyze the influence of particle diameters, which is not considered in the uncertainty evaluation.

In Fig. 7(a) and (b), the measurement results for the default and increased temperature jet flow are compared to the simulated error calculated by Eq. (4), respectively. The temporal fluctuations of the measurements due to the turbulent flow are averaged over 100 individual measurements. The error bars indicate the uncertainty of the mean values for a coverage factor of $k = 3$. The measured position error in Fig. 7a is maximally 2.6 µm, which is quantitatively confirmed by the simulation, but also shows increased quantitative deviations at $x = -1$ µm. Here, an asymmetric flow condition is not considered in the simulation. The measured position error in the increased temperature distribution (Fig. 7b) shows increased values of almost one order of magnitude due to the increased temperature gradients and the increased distance of $\Delta z = 2$ cm to the center of the flow in the viewing direction of the camera. As a result, the course of the simulated data is qualitatively confirmed. Especially in the regions at $x = \pm 2$ cm with the most significant position errors, the majority of the measuring points are also quantitatively confirmed. Therefore, Eq. (4) is a suitable method to calculate the location dependent particle position error in inhomogeneous refractive index fields.

4.1. Triangulation error for stereoscopic setup

Based on the validated method for the determination of the position error for standard PIV with Eq. (4), the triangulation error for a stereoscopic setup is calculated. Here, the determination of the 3D particle position requires two camera images. In combination with Eqs. (5) and (6), the triangulation error is calculated and compared to the measurement results. For this purpose, the luminous end of the glass fiber is imaged by two cameras. The default hot jet flow is moved in the x-direction through both lines of sight of the cameras, see Fig. 8. The lines of sight of the cameras are $\hat{\vec{k}}_1 = (0.52, 0, 0.85)^T$ and $\hat{\vec{k}}_2 = (-0.44, 0, 0.85)^T$, respectively, which corresponds to an angle between both cameras of 121 °. The distance between the center of the hot jet flow and the fiber end in z-direction amounts to 3.4 cm at $y = 2$ cm above the nozzle exit. The measured particle position $\vec{r}_{\text{P}'}$ is determined by the intersection of the lines of sight of the imaged particle, which are defined by the linear equations

$$z(x) = m_i \cdot x + b_i, \tag{11}$$

where $m_i = \frac{k_{i,z}}{k_{i,x}}$ is the slope and b_i is the axis intercept for the cameras $i = 1, 2$. The axis intercept b_i is calculated by

$$b_i = \xi_{z,i} - m_i \cdot \xi_{x,i}. \tag{12}$$

Equating the lines of sight of the imaged particle, Eq. (11) results in

$$r_{\text{P}',x} = \frac{b_1 - b_2}{m_2 - m_1}. \tag{13}$$

The x-component of the measured particle location $r_{\text{P}',x}$ is inserted in Eq. (11) for the determination of the z-component $r_{\text{P}',z}$. In Fig. 9, the absolute value of the error of the measured particle position in x,z-direction is compared with the simulated data using Eqs. (4)–(6). The simulated data show qualitative agreement with the measured data, which are shown with a coverage factor of $k = 3$ for 100 single measurements. Small deviations between the simulated and measured position errors occur in areas with high slopes due to geometrical deviations in the measurement setup. Hence, the method is suitable for the calculation of the location dependent triangulation error in inhomogeneous refractive index fields.

5. Velocity error

5.1. Implications of position errors on velocity determination

The distortion effects of inhomogeneous refractive index distributions also have impacts on the measured velocity $\vec{v} = \left(v_x, v_y, v_z\right)^T$. For this purpose, the results from Elsinga et al. [5] for the velocity error $\Delta\vec{v} = \left(\Delta v_x, \Delta v_y, \Delta v_z\right)^T$ for standard PIV can be applied

$$\Delta\vec{v} = \left(\vec{\nabla}\vec{\xi}\right)\vec{v} - \left(\vec{\nabla}\vec{v}\right)\vec{\xi}. \tag{14}$$

It consists of two influences. First, the change of the particle position error between the two locations of the particle necessary for the velocity determination $(\vec{\nabla}\vec{\xi})\vec{v}$ leads to an error of the measured velocity. And second, the velocity is determined at a false position. This is considered by the multiplication of the velocity gradient and the position error $(\vec{\nabla}\vec{v})\vec{\xi}$.

5.2. Standard PIV

For the considered default flow, the mean position error ξ_x in x-direction is determined with Eq. (4). At $y = 2$ cm, the mean position error ξ_x and the gradient of the mean position error $\nabla_x\xi_x$ are depicted in Fig. 10. The line of sight of the camera is in z-direction. The mean position error ξ_x is maximally 8.7 µm at $x = \pm 2.0$ cm and $z = 2.95$ cm

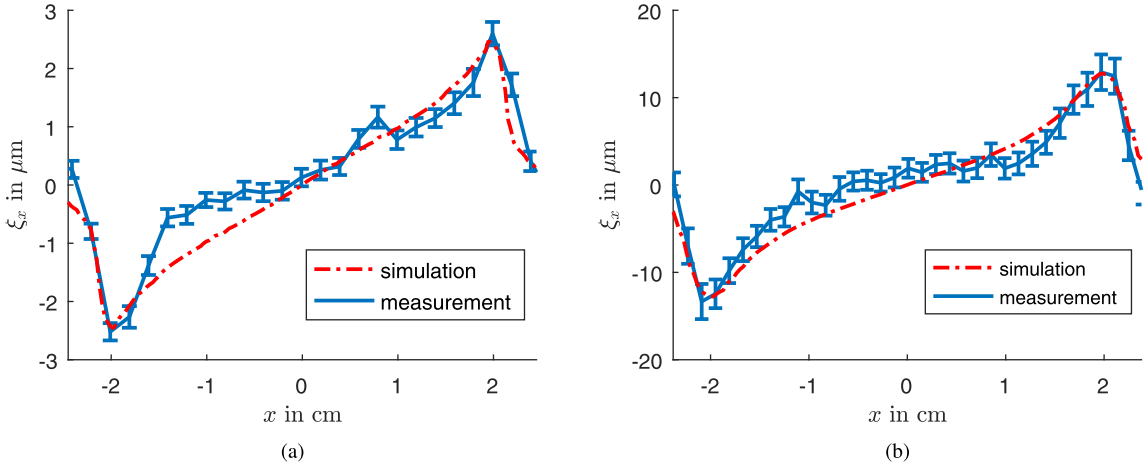

Fig. 7. The measured particle displacement caused by light deflection inside the inhomogeneous refractive index field is compared to simulated results in the hot jet flow. (a) The fiber ending with a diameter of $d_{\text{fiber1}} = 3.4$ µm is moved at $z_{\text{fiber1}} = 1.3$ cm in the default temperature distribution and (b) the fiber ending with a diameter of $d_{\text{fiber2}} = 2.5$ µm is moved at $z_{\text{fiber1}} = 3.3$ cm in the increased temperature distribution.

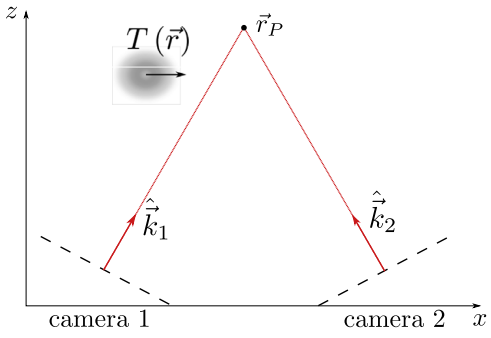

Fig. 8. Experimental setup for the measurement of the triangulation error for a stereoscopic setup due to the influence of an inhomogeneous refractive index distribution which is shifted through the lines of sight $\hat{\vec{k}}_1$, $\hat{\vec{k}}_2$ of the cameras 1 and 2.

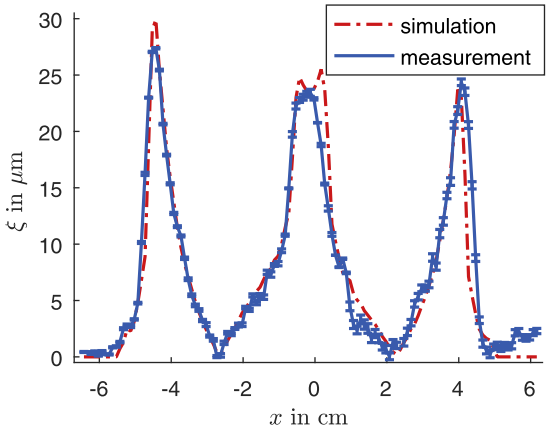

Fig. 9. Simulated and measured error of the absolute amount of the measured particle position in xz-direction by triangulation for a stereoscopic setup.

and the gradient $\nabla_x \xi_x$ of the mean position error is maximally 0.8 % at $x = \pm 2.1$ cm and $z = 2.95$ cm. High temperature gradients in the outer regions of the hot jet flow lead to high errors at $x \approx \pm 2$ cm, which increase linearly in z-direction behind the inhomogeneous temperature distribution.

The relative velocity error is estimated by using the mean spanwise velocity gradients occurring in a jet flow provided by Khashehchi et al. [6]. The resulting relative velocity error consists of

$$\frac{\Delta v_x}{v_x} = 0.8\,\% + 2 \cdot 10^{-5}\,\% \tag{15}$$

at $x = \pm 2.1$ cm and $z = 2.95$ cm. In the examined flow, the first term consisting of the gradient of the particle position error $\nabla_x \xi_x$ is dominant.

5.3. Stereoscopic PIV

The implications of an inhomogeneous refractive index field on the measurement uncertainty for stereoscopic PIV manifest in two different ways. First, as described in Section 5.1, the refractive index field leads to velocity errors for each camera. Therefore, an error calculation is performed to give quantitative information about the measurement error for stereoscopic PIV inside refractive index fields. And second, the stereoscopic self calibration algorithm has increased uncertainties due to the particle position error with triangulation described in Section 3.1.

In stereoscopic PIV measurements, the three components v_x, v_y and v_z of the velocity field are geometrically reconstructed by the two components measurements $\vec{v}_1 = (v_{x,1}, v_{y,1})^T$ and $\vec{v}_2 = (v_{x,2}, v_{y,2})^T$ of each camera with [26]

$$v_x = \frac{v_{x,2}\tan\alpha_1 - v_{x,1}\tan\alpha_2}{\tan\alpha_1 - \tan\alpha_2} \tag{16}$$

$$v_y = \frac{v_{y,2}\tan\beta_1 - v_{y,1}\tan\beta_2}{\tan\beta_1 - \tan\beta_2} \tag{17}$$

$$v_z = \frac{v_{x,2} - v_{x,1}}{\tan\alpha_1 - \tan\alpha_2}, \tag{18}$$

where α_1 and α_2 are the angles between the lines of sight of the cameras and the z-axis in the x,z-plane and β_1 and β_2 are the angles between the lines of sight of the cameras and the z-axis in the y,z-plane. Error propagation of the velocity errors of each camera $\Delta\vec{v}_1 = \left(\Delta v_{x,1}, \Delta v_{y,1}\right)^T$ and $\Delta\vec{v}_2 = \left(\Delta v_{x,2}, \Delta v_{y,2}\right)^T$ relating to the determined velocity components v_x, v_y and v_z leads to

$$\Delta v_x = s_{x,1}\Delta v_{x,1} + s_{x,2}\Delta v_{x,2} \tag{19}$$

$$\Delta v_y = s_{y,1}\Delta v_{y,1} + s_{y,2}\Delta v_{y,2} \tag{20}$$

$$\Delta v_z = s_{z,1}\Delta v_{x,1} + s_{z,2}\Delta v_{x,2}, \tag{21}$$

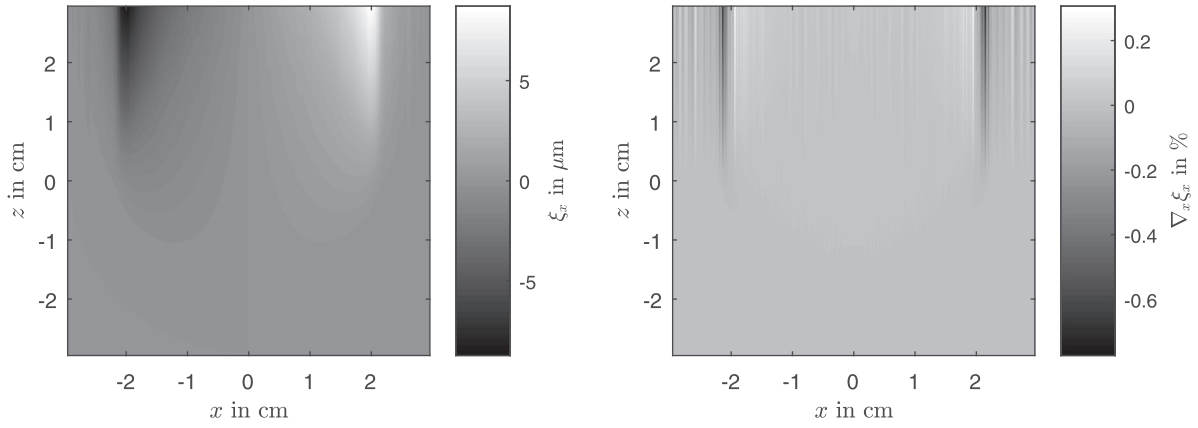

(a) The mean particle position error ξ_x

(b) The gradient of the mean particle position error $\nabla_x \xi_x$

Fig. 10. The mean particle position error ξ_x (a) and its gradient $\nabla_x \xi_x$ (b) inside the hot jet flow in the *x*,*z*-plane at $y = 2$ cm where the line of sight of the camera is in the *z*-direction.

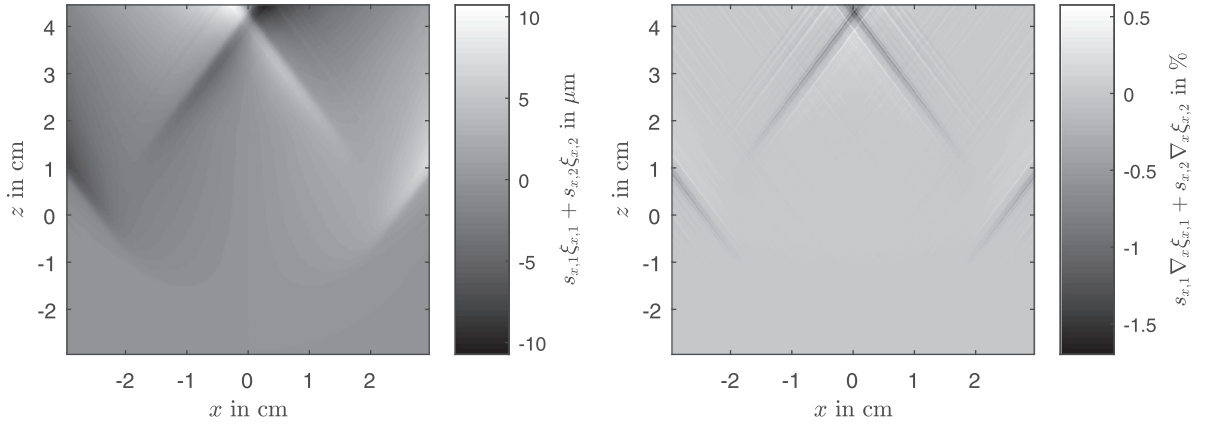

(a) Contribution of the mean position error in *x*-direction

(b) Contribution of the gradient of the mean position error in *x*-direction

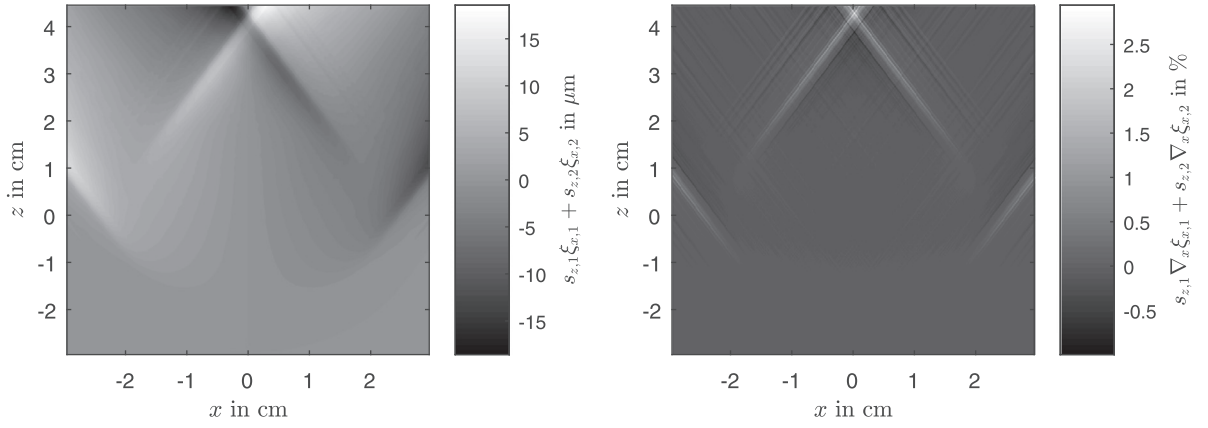

(c) Contribution of the mean position error in *z*-direction

(d) Contribution of the gradient of the mean position error in *z*-direction

Fig. 11. Contributions of the error calculation of the mean particle position errors in *x*-direction (a) and *z*-direction (c) and the gradients of the mean particle position error in *x*-direction (b) and *z*-direction (d) inside the hot jet flow at $y = 2$ cm with stereoscopic PIV. The viewing angles of $\alpha_{1,2} = \pm 30^\circ$ are assumed.

where $\vec{s}_x = \left(\frac{-\tan(\alpha_2)}{\tan(\alpha_1)-\tan(\alpha_2)}, \frac{\tan(\alpha_1)}{\tan(\alpha_1)-\tan(\alpha_2)}\right)^T$, $\vec{s}_y = \left(\frac{-\tan(\beta_2)}{\tan(\beta_1)-\tan(\beta_2)}, \frac{\tan(\beta_1)}{\tan(\beta_1)-\tan(\beta_2)}\right)^T$ and $\vec{s}_z = \left(\frac{-1}{\tan(\alpha_1)-\tan(\alpha_2)}, \frac{1}{\tan(\alpha_1)-\tan(\alpha_2)}\right)^T$ are the sensitivity coefficients of the error contributions. Using Eq. (14) for the quantification of the measured velocity error of each camera $\Delta\vec{v}_1$ and $\Delta\vec{v}_2$, leads to

$$\Delta v_x = \left(s_{x,1}\nabla_x\xi_{x,1} + s_{x,2}\nabla_x\xi_{x,2}\right)v_x + \left(s_{x,1}\xi_{x,1} + s_{x,2}\xi_{x,2}\right)\nabla_x v_x \tag{22}$$

$$\Delta v_y = \left(s_{y,1}\nabla_y\xi_{y,1} + s_{y,2}\nabla_y\xi_{y,2}\right)v_y + \left(s_{y,1}\xi_{y,1} + s_{y,2}\xi_{y,2}\right)\nabla_y v_y \tag{23}$$

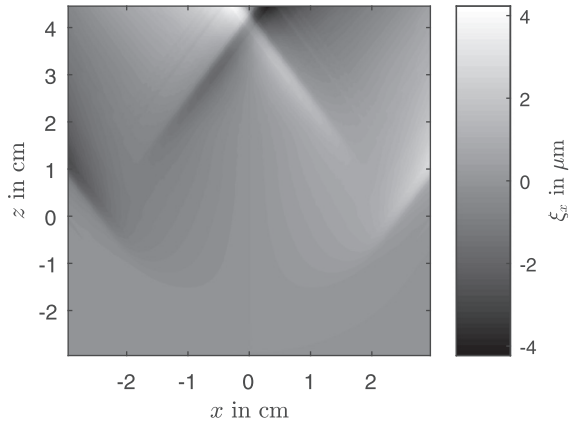

(a) Mean position error in x-direction

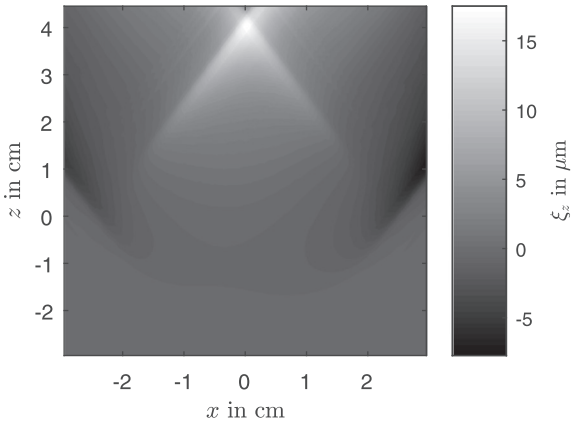

(b) Mean position error in z-direction

Fig. 12. Calculated mean particle position error in (a) x and (b) z-direction inside the hot jet flow at $y = 2$ cm with triangulation. The viewing angles of $\pm 30°$ are assumed.

$$\Delta v_z = \left(s_{z,1}\nabla_x\xi_{x,1} + s_{z,2}\nabla_x\xi_{x,2}\right)v_z + \left(s_{z,1}\xi_{z,1} + s_{z,2}\xi_{x,2}\right)\nabla_z v_z. \tag{24}$$

Assuming viewing angles of $\alpha_1 = 30°$ and $\alpha_2 = -30°$, the terms in the brackets of Eqs. (22) and (24) are depicted in Fig. 11 at $y = 2$ cm in the hot jet flow. The gradient contributions in the first brackets is up to 1.7 % in x-direction and 2.9 % in z-direction at the overlap of the lines of sight through regions with high temperature gradients at $z = 4.3$ cm and $x = 0$ cm. Here, the overlap leads to an intensification of the gradient error contributions, whereas for the contributions of the mean position error the overlap reduces the velocity error contributions. For an estimation of the relative velocity error, the same velocity gradient as for standard PIV is assumed and results in

$$\frac{\Delta v_x}{v_x} = -1.7\,\% + 3 \cdot 10^{-11}\,\% \tag{25}$$

$$\frac{\Delta v_z}{v_z} = 2.9\,\% + 3 \cdot 10^{-11}\,\%. \tag{26}$$

As with standard PIV, the first term of the error calculation is dominant. The results show a significant increase of error for stereoscopic PIV compared with standard PIV with maximal $\frac{\Delta v_x}{v_x} = 0.9\,\% + 3 \cdot 10^{-5}\,\%$ at the same distance from the center of the flow.

The second implication on the measurement error for stereoscopic PIV affects the stereoscopic self calibration algorithm. The stereoscopic self calibration algorithm corrects the calibrated light sheet position by a least square fit through the triangulated particle positions. Therefore, the mean particle position error in x and z-direction with triangulation is calculated with Eqs. (4)–(6) at $y = 2$ cm and depicted in Fig. 12. The overlap at $x = 0$ cm and $z = 4.3$ cm of the lines of sight through regions with high temperature gradients results in an intensification of the error in z-direction and compensates the error contributions in x-direction. The particle position error leads to a systematic error in the correction of the light sheet position by the stereoscopic self calibration algorithm. The calculated position errors can be used for an improved correction of the light sheet.

5.4. Tomographic PIV

For tomographic PIV, which is usually performed with at least four cameras, the considered two camera problem expands to a many camera problem. If each line of sight of the cameras imaging the particle intersects at the position, $\vec{r}_\mathrm{p}$, the approach described in Section 3.1 is suitable. However, large individual particle position errors can lead to divergence of the lines of sight depicting the particle. Wieneke [25] proposed a self calibration method to correct the mapping functions of the cameras in order to achieve convergence of the lines of sight of the cameras imaging the particles. Particle images are used to determine a disparity vector field $\vec{d}_i(\vec{r}) = \left(d_{i,x}(\vec{r}), d_{i,y}(\vec{r}), d_{i,z}(\vec{r})\right)$ for each camera i to match the measured particle positions. In Fig. 13, a visualization of disparities of particle images in an inhomogeneous refractive index distribution is depicted. The disparities for a particle are determined by the minimization of the sum of the individual disparities. In general, an error of the measured particle position remains. A quantification of the particle position error for tomographic PIV can be calculated with Eq. (5) by adding the known disparities

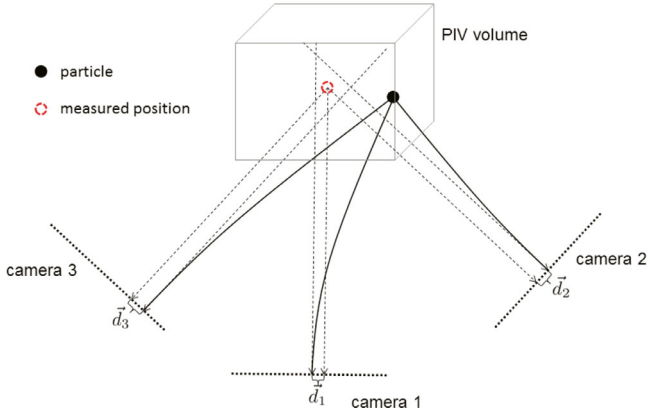

Fig. 13. An inhomogeneous refractive index distribution leads to errors of the particle images for each camera $i = 1, 2, 3$. A determination of the minimal disparities $\vec{d}_i$ allows a reconstruction of the particles position. Generally, an error of the measured position to the true position remains.

$$\vec{\xi} = \vec{\xi}_i + c_i\hat{\vec{k}}_i + \vec{d}_i. \tag{27}$$

No disparities occur in a two camera setup with neglected position error in y-direction. Thus, quantitative information about the velocity error for tomographic PIV inside the hot jet flow are determined for two cameras with viewing angles of $\alpha_1 = 30°$ and $\alpha_2 = -30°$. The position errors for tomographic PIV equal the errors shown in Fig. 12. Discrepancies between the lines of sight of a particle smaller than a pixel already have large impacts on the tomographic reconstruction [4]. Thus, additional position errors in y-direction would reduce the quality of the reconstructed particle positions. In Fig. 14, the gradients $\nabla_x\xi_x$ and $\nabla_z\xi_z$ of the mean particle position errors in x and z-direction at $y = 2$ cm are depicted. As described in Section 5.3 regarding Fig. 12, the overlap at

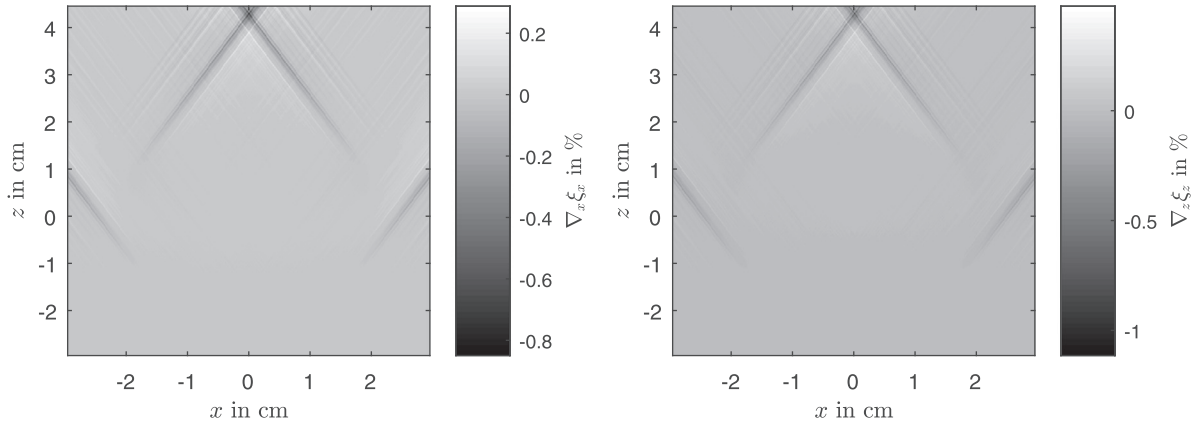

(a) Gradient $\nabla_x \xi_x$ of the mean particle position error in x-direction (b) Gradient $\nabla_z \xi_z$ of the mean particle position error in z-direction

Fig. 14. Calculated gradients (a) $\nabla_x \xi_x$ and (b) $\nabla_z \xi_z$ of the mean particle position error in x and z-direction inside the hot jet flow at $y = 2$ cm with triangulation. The presumed viewing angles are $\alpha_{1,2} = \pm 30\,^\circ$.

$z = 4.3$ cm and $x = 0$ cm of the lines of sight through regions with high temperature gradients results in an intensification of the distinct causes of error. Here, the relative velocity errors for tomographic PIV are increased. Again, the relative velocity error is estimated by using the mean spanwise velocity gradient occurring in a jet flow provided by Khashehchi et al. [6]. The resulting relative velocity errors for tomographic PIV at $z = 4.3$ cm and $x = 0$ cm consist of

$$\frac{\Delta v_x}{v_x} = -0.8\,\% + 1 \cdot 10^{-17}\,\% \tag{28}$$

$$\frac{\Delta v_z}{v_z} = -1.1\,\% + 3 \cdot 10^{-5}\,\% \tag{29}$$

where the first terms are dominant for the examined flow. The results show, that the area affected by measurement errors has increased significantly compared to standard PIV measurements. In addition, the individual errors of the cameras can also have increasing effects on each other.

6. Conclusion

The influence of inhomogeneous refractive index distributions on PIV measurements leads to errors in the measured particle position. Theoretical investigations of the particle position error verify a dependency on the curvature of the refractive index for triangulation, which is performed in stereoscopic and tomographic PIV measurements. For standard PIV, the error only depends on the gradient of the refractive index. The proposed method for the calculation of the particle position error inside refractive index distributions is validated by the comparison with experimental results. For this, the refractive index fields of two hot jet flows with temperatures of up to 191 °C and 291 °C are determined by the measured mean temperature distribution. Furthermore, a method for the calculation of resulting position errors for triangulation is validated by the comparison of simulation and measurement results. For Standard PIV measurements inside the hot jet flow with a maximum temperature of 191 °C, the maximal position error at a distance of the nozzle diameter $d_{\text{nozzle}} = 4.2$ cm in the viewing direction of the camera from the center of the flow and $0.48 d_{\text{nozzle}}$ above the nozzle exit is 12.4 µm. The triangulated position error with viewing angles of $\pm 30\,^\circ$ shows a local maximum of 17.3 µm at a distance of d_{nozzle} from the center of the flow and $0.48 d_{\text{nozzle}}$ above the nozzle exit. Here, the lines of sight through regions with high temperature gradients intercept at this position which leads to increased position errors for triangulation.

The implications of the particle position error on the determined velocity leads to a relative error of 0.9 % in lateral direction of the flow with standard PIV. Error propagation shows velocity errors for stereoscopic PIV of 1.7 % for the lateral in plane velocity and 2.9 % for the out of plane velocity. The velocity determination for triangulated particle positions performed in tomographic PIV shows relative velocity errors of 0.8 % in lateral direction and 1.1 % perpendicular to the lateral direction and the main flow direction. The error estimations are indicated for the same distances of d_{nozzle} from the center of the flow to provide comparability. The estimated errors may be reduced by an averaging effect due to the interrogation window size in the PIV image analysis, whereas for particle tracking velocimetry, this averaging effect does not occur. Furthermore, the provided errors are maximal errors which should be avoided by selecting suitable measurement areas and camera setups to avoid high refractive index gradients in the optical paths from the cameras to the measurement volume. Especially for stereoscopic and tomographic PIV, measurement volumes may arise, where increased individual errors for various cameras lead to an intensification of the measurement error.

As a result, the mean measurement errors for PIV measurements in the examined hot jet flow with a maximum temperature of 191 °C are relative small compared to the overall uncertainty as various studies show [9,10,21–23] but depending on the measurement volume, a measurement uncertainty contribution is generated, which must be taken into account. However, for larger refractive index fields and for higher gradients of the refractive index, the measurement error will rise significantly. In order to give an estimation of the occurring mean velocity errors in higher temperature fields, the temperature profile of the examined hot jet is upscaled to a maximum of 1219 °C, as it occurs in e.g. flame flows. The determination of the refractive index field by Eq. (1) and the determination of the location depending position error for standard PIV with Eq. (4) allows a prediction of occurring mean velocity errors with Eq. (14). For stereoscopic and tomographic PIV, the individual position errors of each camera are calculated with Eq. (4) and inserted into Eqs. (22)–(24) for stereoscopic evaluation or Eqs. (5) and (6) for tomographic reconstruction, respectively. In all cases, the increased temperature field leads to a factor of over two for the mean velocity errors. Here, the influence of the gradient of the mean velocity field is neglected, cf. Eq. (14) second term.

The proposed method does not involve the influence of turbulence. In turbulent flows, an increase of the instantaneous gradient fields of the refractive index occur, as the fluctuations of the particle position error inside the hot jet flow show. Therefore, the resulting velocity error in the instantaneous field will increase. Further, for high Reynolds numbers, the velocity gradients in the instantaneous velocity field are much larger than in the mean field [20]. So, the velocity error in the instantaneous field further increases in comparison to the mean velocity error. In order

to take the influence of turbulence into account, extended investigations of the fluctuating refractive index field and the consideration by the model are necessary, which remains an open task.

In principle, the presented results allow a correction of the measured mean velocity field influenced by the refractive index field. Furthermore, for tomographic PIV, also the influences of the camera numbers and the self calibration algorithm are remaining questions.

References

[1] Adrian RJ. Twenty years of particle image velocimetry. Exp Fluids 2005;39(2):159–69.
[2] Beresh SJ, Wagner JL, Smith BL. Self-calibration performance in stereoscopic PIV acquired in a transonic wind tunnel. Exp Fluids 2016;57(4):48.
[3] Born M, Wolf E. Principles of optics. Pergamon Pr; 1981.
[4] Elsinga GE, Scarano F, Wieneke B, van Oudheusden BW. Tomographic particle image velocimetry. Exp Fluids 2006;41(6):933–47.
[5] Elsinga GE, van Oudheusden BW, Scarano F. Evaluation of aero-optical distortion effects in PIV. Exp Fluids 2005;39(2):246–56.
[6] Khashehchi M, Elsinga GE, Ooi A, Soria J, Marusic I. Studying invariants of the velocity gradient tensor of a round turbulent jet across the turbulent/nonturbulent interface using tomo-PIV. 15th Int symp on applications of laser techniques to fluid mechanics; 2010.
[7] Koukourakis N, Fregin B, König J, Büttner L, Czarske JW. Wavefront shaping for imaging-based flow velocity measurements through distortions using a Fresnel guide star. Opt Express 2016;24(19):22074.
[8] Kühn M, Ehrenfried K, Bosbach J, Wagner C. Feasibility study of tomographic particle image velocimetry for large scale convective air flow. 14th Int symp on applications of laser techniques to fluid mechanics; 2008.
[9] Lawson NJ, Wu J. Three-dimensional particle image velocimetry: experimental error analysis of a digital angular stereoscopic system. Meas Sci Technol 1997;8(12):1455.
[10] Megerle M, Sick V, Reuss DL. Measurement of digital particle image velocimetry precision using electro-optically created particle-image displacements. Meas Sci Technol 2002;13(7):997.
[11] Merzkirch W. Flow visualization. Academic Press; 2012.
[12] Prasad AK. Stereoscopic particle image velocimetry. Exp Fluids 2000;29(2):103–16.
[13] Prasad AK, Adrian RJ. Stereoscopic particle image velocimetry applied to liquid flows. Exp Fluids 1993;15(1):49–60.
[14] Richard H, Raffel M. Principle and applications of the background oriented schlieren (BOS) method. Meas Sci Technol 2001;12:1576–85.
[15] Scarano F. Tomographic PIV: principles and practice. Meas Sci Technol 2013;24(1):012001.
[16] Schlüßler R, Czarske J, Fischer A. Uncertainty of flow velocity measurements due to refractive index fluctuations. Opt Lasers Eng 2014;54:93–104.
[17] Soloff SM, Adrian RJ, Liu Z-C. Distortion compensation for generalized stereoscopic particle image velocimetry. Meas Sci Technol 1997;8(12):1441–54.
[18] Stella A, Guj G, Giammartini S. Measurement of axisymmetric temperature fields using reference beam and shearing interferometry for application to flames. Exp Fluids 2000;29(1):1–12.
[19] Stella A, Guj G, Kompenhans J, Raffel M, Richard H. Application of particle image velocimetry to combusting flows: design considerations and uncertainty assessment. Exp Fluids 2001;30(2):167–80.
[20] Tennekes H, Lumley JL. A first course in turbulence. The MIT Press; 1972.
[21] Voges M, Beversdorff M, Willert C, Krain H. Application of particle image velocimetry to a transonic centrifugal compressor. Exp Fluids 2007;43(2):371–84.
[22] Voges M, Schnell R, Willert C, Mönig R, Müller MW, Zscherp C. Investigation of blade tip interaction with casing treatment in a transonic compressor–part I: particle image velocimetry. J Turbomach 2010;133(1):011007–011007–11.
[23] Westerweel J. Fundamentals of digital particle image velocimetry. Meas Sci Technol 1997;8(12):1379.
[24] Wieneke B. Stereo-PIV using self-calibration on particle images. Exp Fluids 2005;39(2):267–80.
[25] Wieneke B. Volume self-calibration for 3d particle image velocimetry. Exp Fluids 2008;45:549–56.
[26] Willert C. Stereoscopic digital particle image velocimetry for application in wind tunnel flows. Meas Sci Technol 1997;8(12):1465.